

Memo 58

Attenuation of unwanted signals from a moving interferer

M.A. Voronkov, M.H. Wieringa
02/05

Abstract

In this memo we present a study of the attenuation of the radio frequency interference provided by the SKA core in the case of moving interferer (e.g. an aircraft). Identical simulations were carried out for both the Large N (a number of antennae) – Small D (diameter of antennae) and the Small N – Large D designs. The former design provides only a few dB greater attenuation. The attenuation of the signal of a moving interferer (for a short duration and reasonable correlator averaging times and interferer’s speeds) is up to 10 dB better than in the stationary case, but depends on the direction of the motion. Therefore, we recommend using the figures for the stationary case for design and site selection purposes.

1 Introduction

Radio Frequency Interference (RFI) is an important issue for next generation radiotelescopes like the Square Kilometre Array (SKA). Its great sensitivity means it will be vulnerable to unwanted emissions. Efforts are underway to minimize these by proper site selection and appropriate restrictions on radio transmissions in its immediate vicinity. Fortunately, radio interferometers are less susceptible to interference than single dishes because they measure the correlation of signals at two distant locations (e.g. Thompson 1982). In most cases, the phases of the unwanted signal will behave differently from that of the astronomical source and, therefore, the unwanted signal will

decorrelate. This additional attenuation provided by interferometers was studied by Perley (2002) by simulating of a source at the pole followed by imaging of the sky at the declination of interest. In this memo we attempt to give a more accurate formalism to simulate this attenuation and to estimate the degree of such attenuation in the case of moving interferer (e.g. an aircraft).

2 A model of RFI

In our model the unwanted signal was assumed to be a spherical wave emitted from the location specified by the \vec{R}_r vector. The amplitude of the spherical wave was chosen to give a flux density equal to F at the position of the array core specified by the \vec{R}_c vector. In the case of infinitesimal small bandwidth and integration time the response of the phase-tracking interferometer, V_{12} , at each particular time is

$$V_{12} = \frac{F |\vec{R}_r - \vec{R}_c|^2}{|\vec{R}_r - \vec{r}_1| \cdot |\vec{R}_r - \vec{r}_2|} \exp \left\{ \frac{2\pi i}{\lambda} \left(|\vec{R}_r - \vec{r}_1| - |\vec{R}_r - \vec{r}_2| - w \right) \right\}, \quad (1)$$

where \vec{r}_1 and \vec{r}_2 are the positions of antennae for a given baseline, w is the component of the baseline in the direction of the phase centre (phase-tracking interferometer) and λ is the wavelength observed. A derivation of the latter formula is very similar to that of the spatial coherence function of the electric field (e.g. Clark 1999). A basic interferometer response to an astronomical source can be obtained from (1) using the far-field approximation. It follows immediately from (1) that the response to interference does not equal the response to a point source at the pole, as it was simulated by Perley (2002). If the interferer is rather distant so that one can use the far-field approximation, the interferometer response at each particular time will be close to the response to a point source in the direction of interferer, rather than in the direction of either pole, similarly to an ordinary astronomical source. In the near-field case the situation is more complicated. Due to the wavefront curvature the image will be severely distorted. For long observations the time dependence of w becomes important. If the phase centre is at the pole, w remains constant and V_{12} does not change with time provided the position of interferer is fixed with respect to the Earth. For any other location of the phase centre, V_{12} oscillates in time and the signal decorrelates when several visibilities from close baseline spacings, but different times, are averaged together by the gridding routine. A similar decorrelation is caused by time-average smearing due to a finite correlator averaging time. Therefore the interference signal is brighter in an image of the polar region than in an image of the equator, but it does not appear as a point source in either. It is

worth to note, however, that due to the Rayleigh’s theorem for the Fourier transform the ”point source at the pole” approach gives similar results because the phase properties of gridded visibilities do not affect the rms.

Another effect which was not considered by Perley (2002) is time-average smearing. It arises because the phase term in the exponent in (1) is variable in time due to both diurnal rotation of the Earth and the motion of the interferer. Time dependence of the amplitude term reflects the signal becoming stronger or fainter at appropriate antennae. However, this is a second order effect if the distance travelled by interferer during a single correlator integration cycle is small compared to the distances from the antennae. The case, where the interferer, e.g. a plane, is moving very close to the array, can not last long and, thus, is less important. Therefore, we simulated time-average smearing using the following formula, which takes into account the phase term only and implies a linear dependence on time within a single integration cycle of the correlator,

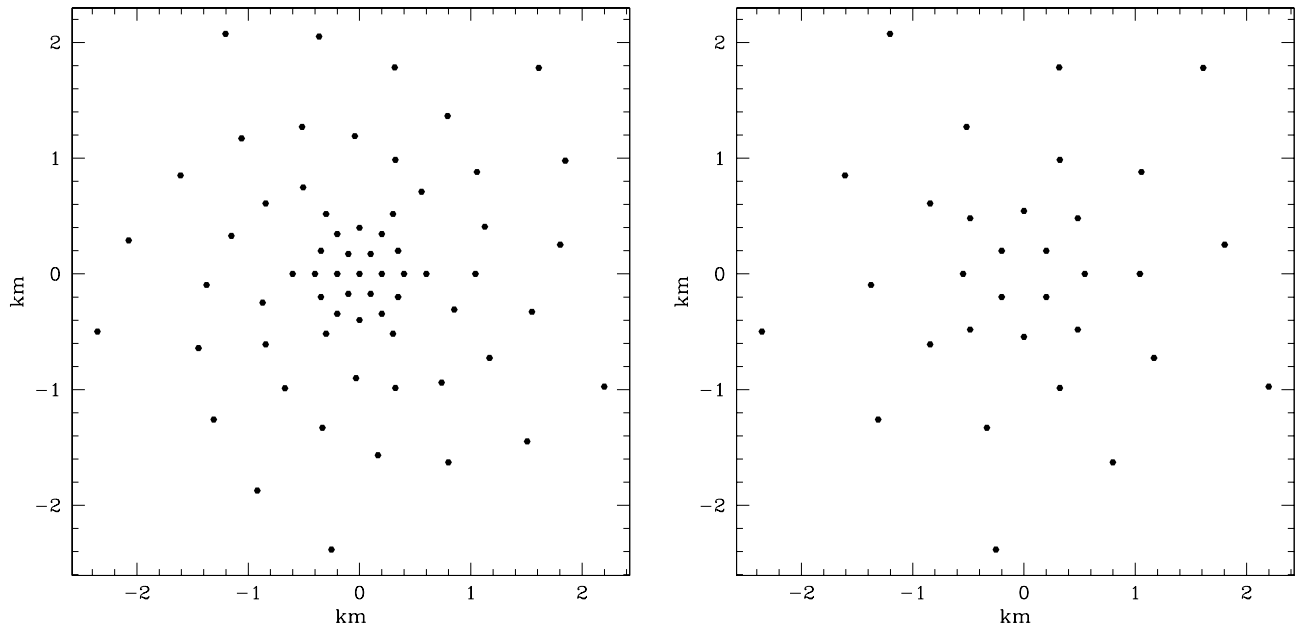
$$\widetilde{V}_{12} = V_{12} \operatorname{sinc} \left\{ \frac{\pi}{\lambda} \left[\left(\frac{\vec{R}_r - \vec{r}_1}{|\vec{R}_r - \vec{r}_1|} - \frac{\vec{R}_r - \vec{r}_2}{|\vec{R}_r - \vec{r}_2|} \right) \dot{\vec{R}}_r - \dot{w} \right] \tau \right\}, \quad (2)$$

where τ is the correlator averaging time, $\dot{\vec{R}}_r$ is the velocity vector of the interferer, and \dot{w} is the rate with which w is changing due to diurnal rotation of the Earth.

3 Simulations

All simulations were carried out in the AIPS++ environment¹ using the formulae described above for various averaging times, interferer speeds, and declinations. The simulations were done for two layouts representing the large N (number of antennae) – small D (diameter of antennae) design (hereafter, LNSD), which included 65 stations, and the small N – large D design (hereafter, SNLD), which included 32 stations (Fig. 1). Both these layouts were given as templates in the guidelines for site proposers. Because the interference response is stronger at short baselines we simulated only the array core and its immediate vicinity (core plus central area, <3km from the centre as shown in Fig. 1). The imaging stage involved no deconvolution. All images were 1024×1024 pixels, the pixel size was 4”. Uniform weighting was used. The attenuation was calculated as the ratio of the flux density F of the interfering signal to the rms noise level in

¹The AIPS++ software package is developed by the National Radio Astronomy Observatory (NRAO), which is a facility of the National Science Foundation operated under cooperative agreement by Associated Universities, Inc.



(a) The Large N – Small D design (LNSD).

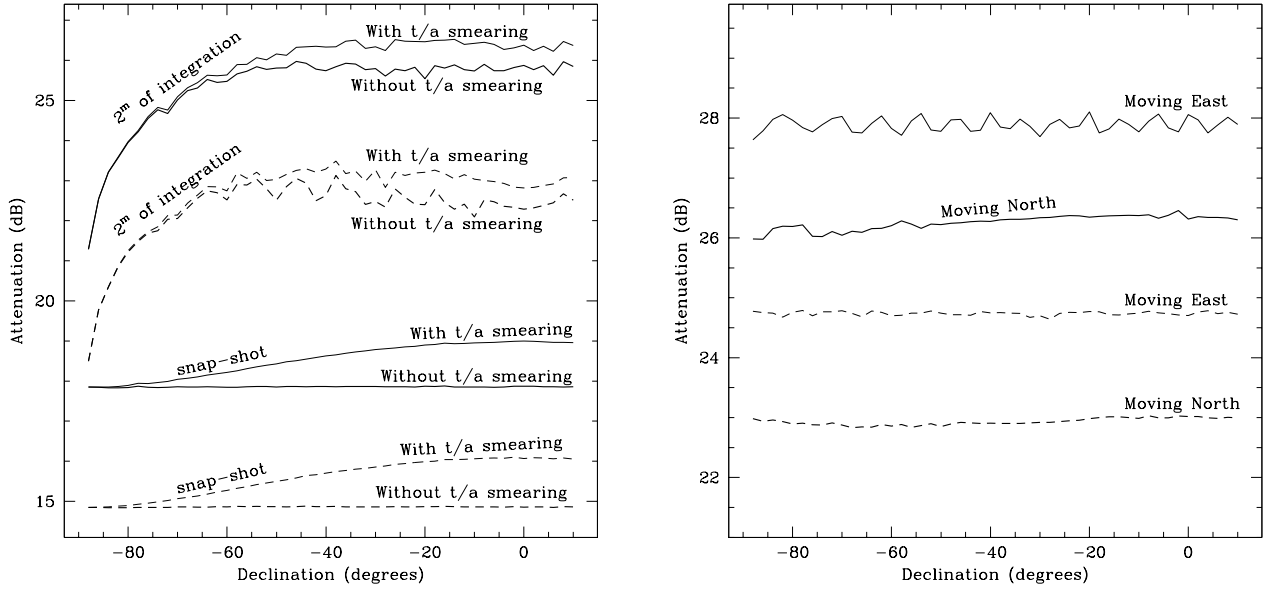
(b) The Small N – Large D design (SNLD).

Figure 1: Array layouts used for simulations from the guidelines for site-proposers. The center of both layouts is assumed to be at -29.8 degrees of latitude.

the dirty image. Most simulations were done assuming snapshot observations (only one visibility per baseline) and a correlator averaging time of 1 second (i.e. time-average smearing was simulated). However, in the case of a stationary interferer we simulated models with infinitesimal small correlator averaging time (i.e. no time-average smearing) as well as models with 2 minutes of observations (i.e. 120 correlator integration cycles) in addition to the models mentioned above. No bandwidth smearing was simulated because the SKA is expected to have high spectral resolution. The frequency was assumed to be 1.4 GHz for all models. No attenuation due to the primary beam was simulated as it requires additional knowledge of the antenna design, although the interference signals are unlikely to enter through the the main lobe. In practice, this will further attenuate unwanted signals.

4 Results and discussion

The dependence of attenuation on the declination of the phase centre for the stationary and moving interferer is shown in Fig. 2. In both cases the attenuation is greater for the



(a) The case of stationary interferer with and without time-average smearing. Results for a snapshot (one visibility per baseline) and for a 2 minute integration are shown.

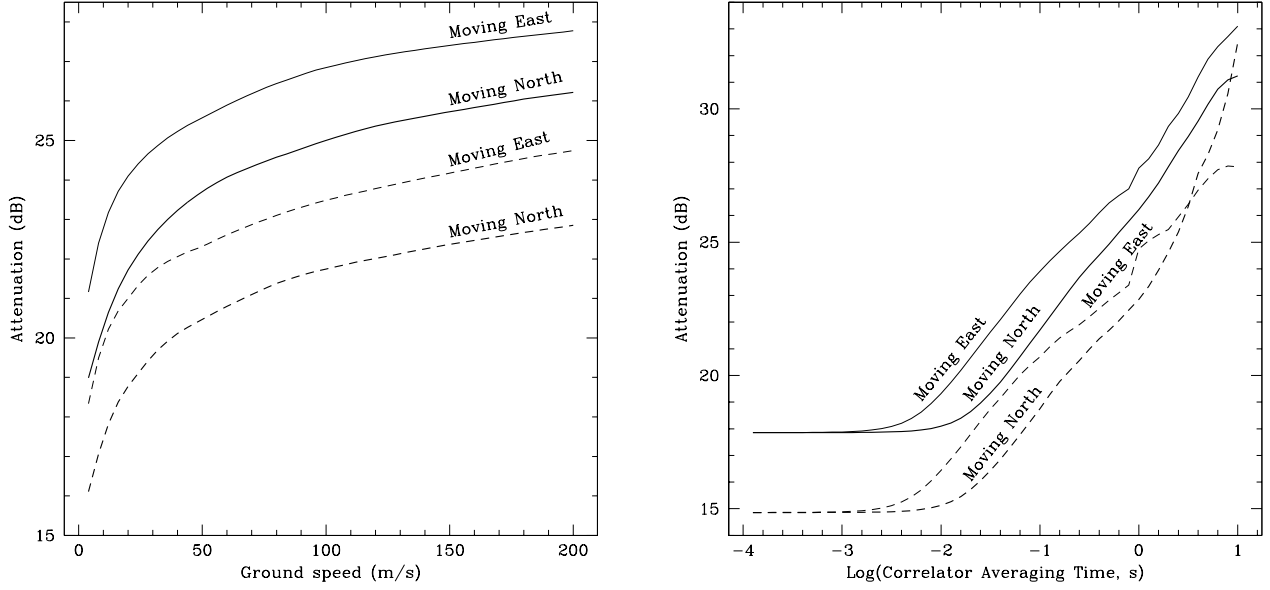
(b) The case of moving interferer (the ground speed is 200 m s⁻¹). Snap-shot (one visibility per baseline) observations. Correlator averaging time is 1 s.

Figure 2: The attenuation of unwanted signal by interferometer versus the declination of the phase centre. The interferer is located 10' of latitude North from the array core and 13 km above the ground. The LNSD results are shown by the solid lines, dashed lines represent the SNLD results.

LNSD design. This is expected because a larger number of antennae produces more visibilities. For snapshot observations without time-average smearing, the attenuation is simply $10 \log N$, where N is the number of antennae. For longer integrations additional attenuation arises from incoherent averaging of visibilities within a uv -cell due to the phase rotation of a tracking interferometer. Perley (2002) has studied this effect of the fringe-winding attenuation in detail and derived an approximate formula estimating the effect (see equation 10 in that paper). It can be expressed in decibels as

$$\text{Attenuation(dB)} = 6.8 + 10 \log N + 5 \log(t(\text{sec}) B_m(\text{km}) \cos \delta) - 5 \log \lambda(\text{cm}), \quad (3)$$

where $t(\text{sec})$ is the duration of observations (interference has the same duration) in seconds, δ is the declination of the phase centre, $\lambda(\text{cm})$ is the observed wavelength in centimetres, B_m is a "mean" baseline length. This mean baseline length is determined



(a) The attenuation versus the ground speed. Correlator averaging time is assumed to be 1s.

(b) The attenuation versus the correlator averaging time. Ground speed is assumed to be 200 m s^{-1} .

Figure 3: The dependence of the attenuation at -50° declination on the ground speed and the correlator averaging time. Solid and dashed lines represent the LNSD and SNLD layouts, respectively.

by the formula

$$B_m = \left(\frac{2}{N(N-1)} \sum_{i=1}^{\frac{N(N-1)}{2}} \frac{1}{B_i} \right)^{-1}, \quad (4)$$

where B_i is an individual baseline. For the studied layouts B_m are 1.1 km and 1.3 km for the LNSD and SNLD designs, respectively. For equatorial observations at 1.4 GHz, with 2 minutes of integration, equation (3) yields the attenuation of 28.9 dB and 26.2 dB for the LNSD and SNLD cases. Both values are a few dB higher than the result of simulations shown in Fig. 2. This discrepancy is below the accuracy expected from the approximate formula (see Fig.6 from Perley, 2002).

A decorrelation similar to that described above occurs at the correlator if the correlator averaging time is finite (time-averaging smearing), but according to Fig. 2a this effect is small. The effect is difficult to analyse analytically because the orientation of individual baselines is important. In the case of a moving interferer, the effect of time-

average smearing becomes even more complex as an additional term depending on the velocity of interferer and the direction of its motion appears in equation (2). Fig. 2b shows the results for the cases of eastward and northward motion of the interferer from the array core. The attenuation is up to 10 dB higher than in the case of the stationary interferer. The dependence of the attenuation on the interferer's speed and the correlator averaging time is shown in Fig. 3. For reasonable averaging times less than 1 s and subsonic speeds the attenuation is not greater than 10 dB above the value in the stationary case.

The snapshot case is an attractive model for these calculations because it depends neither on the trajectory of interferer, nor on the amplitude variations with time. This greatly reduces the dimensionality of parameter space. However, to get figures for more realistic cases we simulated a 2 minute integration (interferer travelled 24 km at 200 m s^{-1}) at -50° declination for various orientations of a linear trajectory (including overflying of the array core at the altitude of 10 km). For each correlator cycle we computed a new position of the interferer \vec{R}_r using the velocity vector $\dot{\vec{R}}_r$. The attenuation is up to 10 dB greater than in the stationary case with 2 minute integration shown in Fig. 2a and also depends on the direction of motion of the interferer. So, the same result applies as in the snapshot case. However, for some trajectories (mainly when the interferer is seen at low elevation from the array core centre and is moving to the north) this additional attenuation was very small and the total attenuation was almost equal to the stationary case (with 2 minute integration). At distances of more than a few tens of kilometers from the core centre the total effect is close to that in the stationary case. Taking into account that a radio quiet zone and a restricted area for flying will most likely be established in the vicinity of the SKA core, we recommend to use the most conservative estimate obtained in the case of the stationary interferer (equation (3) or Perley (2002) results).

5 Conclusions

1. The Large N – Small D (LNSD) design layout attenuates unwanted signals better than the Small N – Large D (SNLD) design layout, but the difference is a few dB only.
2. The attenuation of the signal of a moving interferer is typically up to 10 dB better than that of a stationary source for reasonable correlator averaging times, duration of experiment and subsonic speeds. The effect depends on the trajectory of the interferer and sometimes is rather small. Therefore, we recommend using the figures for the stationary case for array design and site selection purposes.

References

- Clark B.G., Coherence in Radio Astronomy, 1999, ASP Conf. Ser., G.B. Taylor, C.L. Carilli and R. A. Perley (eds.), 180, 1
- Perley R., Attenuation of Radio Frequency Interference by Interferometric Fringe Rotation, 2002, EVLA Memo 49
- Thompson A.R., The Response of a Radio-Astronomy Synthesis Array to Interfering Signals, 1982, IEEE Transactions on antennas and propagation, 30, 450